THE JOURNAL OF PHYSICAL CHEMISTRY A

ARTICLE

pubs.acs.org/JPCA

Investigation of the Fe K-edge XANES Spectra from $Fe_{1-x}Ga_xSbO_4$: Local versus Nonlocal Excitations

Jessica A. Sigrist, Michael W. Gaultois, and Andrew P. Grosvenor*

Department of Chemistry, University of Saskatchewan, Saskatoon, Saskatchewan, Canada S7N 5C9

ABSTRACT: The Fe K-edge X-ray absorption near-edge (XANES) spectra from $Fe_{1-x}Ga_xSbO_4$, having a rutile-like structure, have been investigated. Similar to the Ti K-edge XANES spectrum from TiO_2 (rutile), the low-energy pre-edge region observed in the Fe K-edge spectra is too broad to be representative of only a local, quadrupolar 1s → 3d excitation. The broadness of this peak results from the presence of a nonlocal transition, referred to as an intersite hybrid, which involves the excitation of 1s electrons to unoccupied 3d states of a next-nearest-neighbor Fe atom. (These 3d states overlap Fe 4p states of the absorbing atom through O 2p states.) With increasing Ga concentration, the intensity of the intersite hybrid peak decreases because of a deficiency of unoccupied next-nearest-neighbor 3d states. This observation provides important information on how the peak intensities of these nonlocal excitations are affected by substitution of the constituent elements.

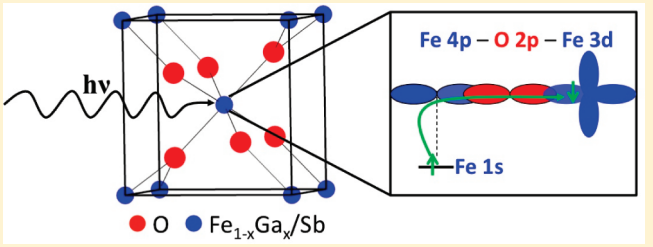

1. INTRODUCTION

To study transition-metal oxides, transition-metal K-edge X-ray absorption near-edge spectroscopy (XANES) has become an invaluable technique to investigate variations in the local coordination environment and electronic structure depending on composition, preparation method, and structure.[1−3] To interpret the K-edge line shape, a molecular-orbital approach is often used, assuming that the absorbing metal atom only interacts with atoms located in the first coordination shell (i.e., all transitions are assumed to be local).[4,5] For example, in the Fe K-edge spectra from $FePO_4$ (Fe is located in a tetrahedral site) and $FePO_4 \cdot xH_2O$ (Fe is located in an octahedral site) presented in Figure 1a, the differences in line shape and absorption energy can be explained by only considering the number of O atoms that directly bond to the Fe center.[6−10] (Within both compounds, P is located in the second coordination shell.[6])

The spectra shown in Figure 1a can be separated into two regions (A and B), which result from quadrupolar (A: Fe 1s → 3d) and dipolar (B: Fe 1s → 4p) excitations, respectively.[1,4,7] The intensity of the lowest energy "pre-edge" peak observed in region A increases considerably with decreasing coordination number (CN) of the metal center (cf. left inset of Figure 1a).[4,7] With loss of inversion symmetry, 4p states partially overlap the 3d states and add a dipolar contribution to the excitation, which results in a stronger pre-edge excitation.[4] (Changes in bond length and charge of the metal center can also affect the intensity of the pre-edge peak.[4,11]) Above the pre-edge peak, the strong main edge, which is a dipolar excitation (region B in Figure 1a; represents Fe 1s → Fe 4p states interacting with O 2p states), decreases in energy and intensity as the CN is lowered. The shift in absorption-edge energy is a result of final-state relaxation effects, while the change in intensity is a result of a change in the number of Fe 4p−O 2p antibonding states available for 1s electrons to be excited to.[7,9,10]

Unlike the phosphates discussed above, not all transition-metal K-edge XANES spectra can be interpreted by examination of the first coordination shell alone (e.g., Fe_2O_3 and TiO_2).[1,11−19] The Fe K-edge spectrum from α-Fe_2O_3 (hematite) is presented in Figure 1b with the background-subtracted pre-edge region presented in the inset. The general features of the main-edge region (B; >7120 eV) are similar to those found in the spectrum from $FePO_4 \cdot xH_2O$ as Fe is also found in an octahedral coordination environment in α-Fe_2O_3 (cf. Figure 1a), but the pre-edge region (A) is significantly broader (see inset of Figure 1b). The line shape of the pre-edge from α-Fe_2O_3 is inconsistent with what might be expected based on examination of the first coordination shell alone: a single broad peak resulting from the excitation of 1s electrons to crystal-field split 3d states (cf. the pre-edge peak from $FePO_4 \cdot xH_2O$ in the inset of Figure 1b).[1] The additional, higher-energy (>7115 eV) intensity corresponds to a nonlocal transition, often referred to as an intersite hybrid.[1,12−14,20−22]

The intersite hybrid excitation described above results from the promotion of a 1s electron to 3d states of a next-nearest-neighbor Fe atom.[13] These 3d states are hybridized with 4p states of the absorbing Fe atom through O 2p states.[13] Owing to the overlap of metal 4p and 3d states, there is a dipolar nature to this

Received: December 3, 2010
Revised: January 24, 2011
Published: February 22, 2011

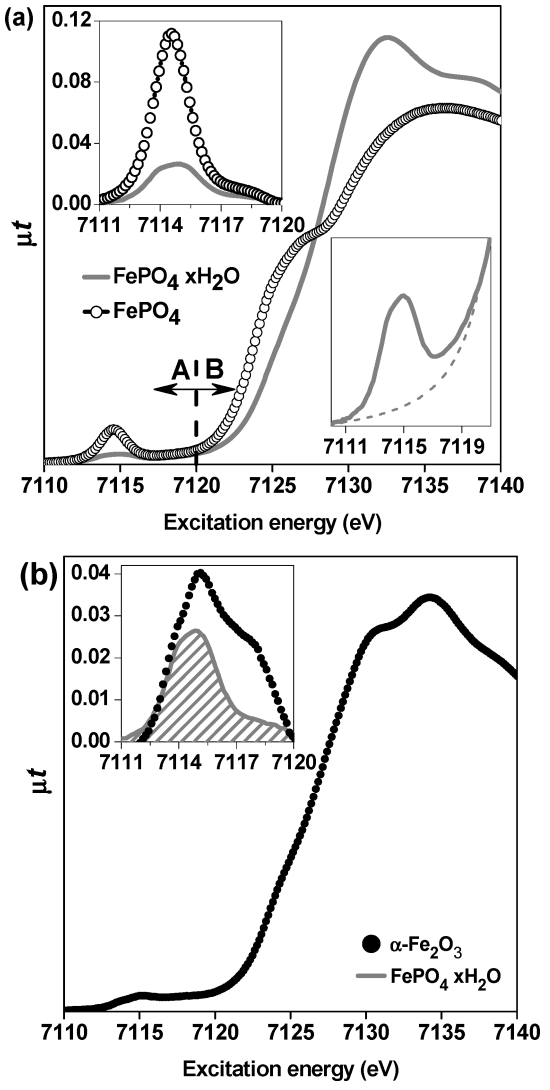

Figure 1. (a) Fe K-edge spectra from $FePO_4 \cdot xH_2O$ and $FePO_4$. To investigate the change in the pre-edge intensity, the spectra were fitted with a background function, representing the leading edge of the higher intensity dipolar region, and its construction is presented in the right-most inset. The change in intensity of the pre-edge intensity with coordination number is shown in the left-most inset. (b) Fe K-edge spectrum from α-Fe_2O_3. The inset shows the background-subtracted pre-edge region of α-Fe_2O_3 versus that from $FePO_4 \cdot xH_2O$.

peak, making it generally more intense than quadrupolar, pre-edge excitations.[13,19,20] Intersite hybrid peak intensities are known to be affected by (i) the metal−O−metal bond angle, (ii) the metal−O bond length, and (iii) the CN of the transition metal.[20,23] The effect of (iii) is a result of the lowering of the CN from 6, leading to the overlap of np and $(n - 1)$d states of the transition-metal center, and reducing the ability of these states to interact with np and $(n - 1)$d orbitals from a next-nearest-neighbor metal atom.[23] As of yet, it is not understood how intersite hybrid peaks are influenced by the average occupancy of the $(n - 1)$d states of the next-nearest-neighbor transion-metal atom. In this study, the Fe K-edge XANES spectra from $Fe_{1-x}Ga_xSbO_4$ are discussed. (These materials adopt a rutile-type structure (Figure 2) in which the concentration of next-nearest-neighbor Fe 3d states can be tuned through substitution.[24,25]) An intersite hybrid peak has been identified in these spectra and has

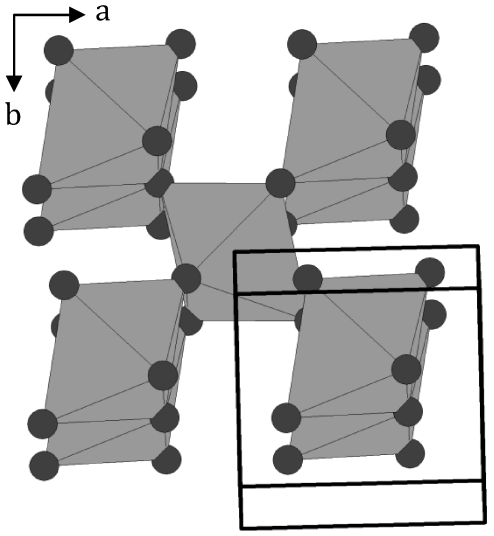

Figure 2. Rutile-type structure of $Fe_{1-x}Ga_xSbO_4$ looking down the c-axis. The tetragonal structure contains edge- and corner-sharing $(Fe_{1-x}Ga_x/Sb)O_6$ octahedra. Within the structure, the Fe^{3+}, Ga^{3+}, and Sb^{5+} cations are randomly distributed in the same crystallographic site.[24]

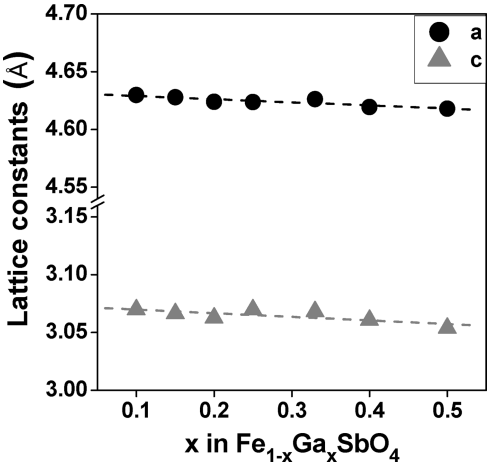

Figure 3. Change in lattice constants (a and c) with increasing Ga content.

allowed for the development of a better understanding of these excitations, and transition-metal K-edge XANES spectra in general.

2. EXPERIMENTAL SECTION

2.1. Synthesis. $Fe_{1-x}Ga_xSbO_4$ ($x = 0.1, 0.2, 0.3, 0.4, 0.5$) was synthesized by stoichiometric reaction of the binary oxides (α-Fe_2O_3, Alfa Aesar, 99.945%; Ga_2O_3, Alfa Aesar, 99.99%; Sb_2O_3, Alfa Aesar, >99%) at 1373 K for >3 days with intermediate grinding. (Longer heating times were required when $x \geq 0.4$.) The purity of the synthesized materials was confirmed by powder X-ray diffraction (pXRD) using a Rigaku Rotaflex RU-200 rotating anode X-ray diffractometer. All materials were found to adopt a tetragonal, rutile-type structure ($P4/mnm$) with purities of 100% for $x \leq 0.3$ and ≥95% for $0.4 \leq x \leq 0.5$. Lattice constants of the $Fe_{1-x}Ga_xSbO_4$ system were determined using the program Unit Cell and were found to decrease somewhat with increasing Ga concentration, a result of the Ga^{3+}

atoms being slightly smaller than Fe^{3+} atoms and in agreement with Vegard's law (Figure 3).[26−28] The magnitude of the decrease in the dimensions of the unit cell is small, implying little change in the O−$Fe_{1-x}Ga_x$/Sb bond lengths with increasing Ga content. $FePO_4$ (anhydrous) was synthesized by reaction of α-Fe_2O_3 and P_2O_5 at 1173 K and was stored under $N_{2(g)}$ in a glovebox. (This anhydrous phosphate was confirmed to be phase-pure by powder diffraction.)

2.2. XANES. Fe K-edge XANES spectra from $Fe_{1-x}Ga_xSbO_4$ were collected at the Canadian Light Source (CLS), using the Hard X-ray Micro-Analysis (HXMA) insertion device beam line, 06ID-1. The flux is ∼6 × 10^{11} photons/s, and the maximum achievable resolution is better than 1 eV at photon energies below 10 keV. Based on the collection of multiple spectra from each material, the precision of the measured absorption energies was determined to be ±0.1 eV. To act as standards, spectra from α-Fe_2O_3, $FePO_4 \cdot xH_2O$ (Alfa Aesar), and $FePO_4$ were also collected. Samples were finely ground and sandwiched between Kapton tape, and transmission spectra were collected using N_2-filled ionization chambers. The thickness of the sample was varied by adding or removing layers of tape to maximize the edge-step height. Spectra were collected from greater than 150 eV below the absorption edge to greater than 500 eV above the absorption edge to ensure proper normalization, and the X-ray energy was increased through the absorption edge by 0.15 eV per step. The spectra were calibrated by setting the maximum of the first derivative of a spectrum from Fe metal collected concurrently in transmission mode to 7112 eV.[29] To study the intensity and line shape of the pre-edge region, the background was fitted using an arc-tangent function having a full-width-at-half-maximum (fwhm) of ∼1.8 eV and a centroid energy of ∼7120 eV to account for the leading edge of the intense, dipolar excitation (main edge). (In the the case of α-Fe_2O_3, the resulting background subtracted pre-edge region (inset of Figure 1b) was similar in line shape to that reported previously.[1,14])

To better understand local transitions involving the excitation of electrons into 3d states, Fe L_3-edge XANES spectra resulting from 2p → 3d transitions were collected from $FePO_4 \cdot H_2O$ and $Fe_{1-x}Ga_xSbO_4$ ($0 \le x \le 0.3$) at the CLS using the spherical grating monochromator (SGM) undulator beam line, 11ID-1. The flux is ∼10^{11} photons/s at 1900 eV and increases to ∼4 × 10^{12} photons/s at 250 eV. The resolution is better than 0.3 eV at photon energies below 1500 eV, and the instrumental precision is better than ±0.1 eV. Powdered samples were mounted on carbon tape and measured in vacuo. Total electron yield (TEY) spectra were collected from ∼30 eV below the absorption edge to ∼50 eV above the edge to get a suitable background for normalization. All spectra were collected with a 0.1 eV step size through the absorption edge. The Fe L_3-edge spectra were calibrated against Fe metal powder with the maximum in the first derivative of the L_3-edge set to 706.8 eV.[29] All XANES spectra were analyzed using the Athena software program.[30]

3. RESULTS AND DISCUSSION

The normalized Fe K-edge spectra from $Fe_{1-x}Ga_xSbO_4$ are presented in Figure 4a and have been separated into two regions, labeled as A and B, in accordance with Figure 1a. With increasing Ga content, the main-edge absorption energy, resulting from a 1s → 4p transition (region B in Figure 3a), shifts to higher energy by ∼0.3 eV over the entire range of substitution (see inset of Figure 4a). Absorption energies can shift because of variations in the charge of the absorbing atom and the identity of the neighboring atoms. Both of these ground-state effects result in a change in the ability of the nuclear charge on the absorbing atom to be screened. Final-state relaxation may also contribute to shifts in absorption energy, but this effect is minor when the CN of the absorbing atom is fixed, as is the case here. In the Fe K-edge

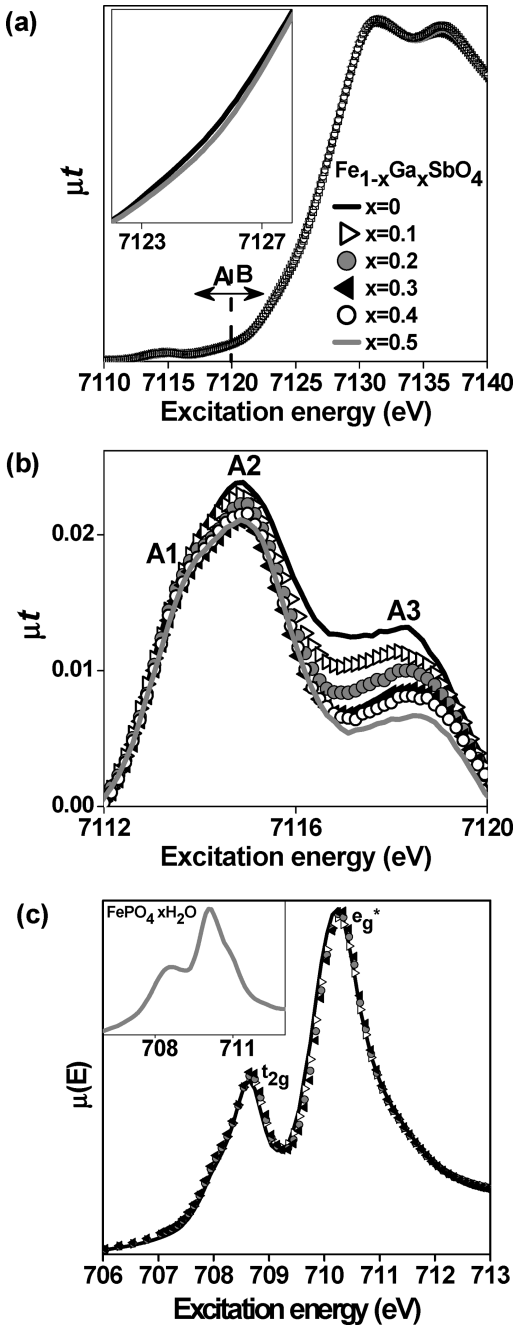

Figure 4. (a) Fe K-edge XANES spectra from $Fe_{1-x}Ga_xSbO_4$ ($0 \le x \le 0.5$). The inset shows an expanded view of the dipolar region of the spectrum (B), which highlights the observed shift in absorption energy. For clarity, only the end members (x = 0, 0.5) are shown in the inset. (b) Background-subtracted pre-edge region (A) from $Fe_{1-x}Ga_xSbO_4$ showing a decrease in intensity of the nonlocal features, A2 and A3, with increasing Ga content. (c) Fe L_3-edge spectra from $Fe_{1-x}Ga_xSbO_4$ ($0 \le x \le 0.3$). The crystal-field split 3d t_{2g} and e_g* states are labeled. The corresponding Fe L_3-edge spectrum from $FePO_4 \cdot xH_2O$ is presented in the inset of (c).

spectra investigated here, the shift in absorption energy can be ascribed to the substitution of Ga for Fe in the Fe−O−M bond. (In this notation, Fe represents the absorbing metal center and M represents its next-nearest-neighbor, $Fe_{1-x}Ga_x$/Sb.) As Ga substitutes for Fe in the same crystallographic site, the average electronegativity of the next-nearest-neighbor elements, M, around the Fe center increases ($\chi_{Fe} = 1.64 < \chi_{Ga,\ Sb} = 1.82$).[24,31] With increasing x, the O−M bond becomes more covalent, which, to ensure balanced charges, leads to the development of a more polar Fe−O bond. As a more polar Fe−O bond is developed with increasing x, the Fe charge becomes more positive. This increase in charge results in reduced ground-state screening of the Fe nuclear charge and is observed as an increase in absorption energy.

Along with a shift in the absorption energy of region B, changes to the lower energy, less intense pre-edge region (A) of the spectra were also observed. The background-subtracted pre-edge region (A) of $Fe_{1-x}Ga_xSbO_4$ is presented in Figure 4b. Similar to the pre-edge region of the Ti K-edge spectrum from TiO_2 (rutile), three features are observed and have been labeled as A1, A2, and A3 (see Figure 4b).[15−18] The lowest energy feature in the inset of Figure 4b, A1, is a quadrupolar transition resulting from the local excitation of 1s electrons to unoccupied 3d states of the absorbing atom. This assignment is based on the similarity in energy of this feature to the pre-edge peak observed in the spectrum from $FePO_4 \cdot xH_2O$ (cf. Figure 1a), and by comparison to experimental and theoretical analyses of the Ti K-edge spectrum from rutile (TiO_2) as well as by examination of the complementary Fe L_3-edge XANES spectra.[15−18]

The Fe L_3-edge spectra from $Fe_{1-x}Ga_xSbO_4$ and $FePO_4 \cdot xH_2O$ are presented in Figure 4c and result from the excitation of 2p electrons to unoccupied 3d conduction states of the same atom. When Fe has an octahedral coordination environment, the Fe L_3-edge spectrum contains two peaks representing the excitation of 2p electrons to the crystal-field split 3d t_{2g} and 3d e_g^* states.[32,33] The excitation investigated in L_3-edge spectra is similar to the local, pre-edge excitation (1s → 3d) observed in some K-edge spectra, although the peak widths can be different because of final-state, core-hole lifetime effects.[34] However, comparison of these spectra can help to determine if a K-edge pre-edge peak *only* contains local interactions. (Here, it is not necessary to also investigate L_2-edge spectra as K-edge excitations do not undergo spin−orbit splitting.) Comparing the Fe K- and L_3-edge spectra from $FePO_4 \cdot xH_2O$ first, the local, 1s → 3d pre-edge excitation in the Fe K-edge spectrum (inset of Figure 1a and 1b) is similar in fwhm to that of the entire Fe L_3-edge spectrum (inset of Figure 4c; 3.0 eV versus 2.8 eV).

The Fe L_3-edge spectra from $Fe_{1-x}Ga_xSbO_4$ are presented in Figure 4c and have a total fwhm (∼2.5 eV) that is significantly more narrow than the fwhm of the pre-edge region observed in the corresponding K-edge spectra (Figure 4b; ∼5.5 eV). This comparison implies that although feature A1 in the Fe K-edge XANES spectra from $Fe_{1-x}Ga_xSbO_4$ (Figure 4b) can be associated with a local, 1s → 3d transition, features A2 and A3 cannot. Instead, the higher energy pre-edge features, A2 and A3, are representative of nonlocal, intersite hybrid transitions. In the case of TiO_2 (rutile), two intersite hybrid peaks (labeled as A2 and A3) are observed because the structure contains both corner- *and* edge-sharing octahedra resulting in the presence of nondegenerate 4p states, which can overlap with next-nearest-neighbor 3d t_{2g} and e_g^* states.[15−17] As $Fe_{1-x}Ga_xSbO_4$ adopts the rutile-type structure (Figure 2), peaks A2 and A3 observed in Figure 4b can be associated with the same interactions. (Similar to TiO_2, A2 also likely contains some contribution from a local, quadrupolar 1s → 3d excitation.[15])

As expected, the intensity of feature A1 in Figure 4b changes very little with increasing Ga concentration because this peak results only from a local excitation (1s → 3d) whose intensity is primarily dependent on CN.[4] In contrast to A1, the intensities of features A2 and A3 decrease considerably with increasing Ga content. In this material, the replacement of Fe^{3+} by Ga^{3+} leads to a slight decrease in the lattice constants (Figure 3), causing an average reduction in the Fe−O−M bond lengths and resulting in increased overlap of the next-nearest-neighbor Fe 3d−Fe 4p states. As observed previously for Co-containing oxides, such a change should result in the development of a more intense intersite hybrid peak, but this is not observed in Figure 4b.[20] In the system investigated here, the decrease in intensity of features A2 and A3 with greater Ga contents is related to the concentration of unoccupied next-nearest-neighbor Fe 3d orbitals. With increasing Ga concentration, fewer next-nearest-neighbor Fe 3d states are available for 1s electrons from the absorbing Fe center to be excited to, and the intersite hybrid peak intensity decreases. The difference in intensity change between A2 and A3 is likely a result of A2 also containing contributions from a local, quadrupolar 1s → 3d transition that is not influenced by the substitution of Fe for Ga.

4. CONCLUSIONS

In this study, the pre-edge region of Fe K-edge XANES spectra from $Fe_{1-x}Ga_xSbO_4$ was found to contain nonlocal, intersite hybrid excitations. For the first time, the intensity of these peaks was observed to be proportional to the average occupancy of the $(n - 1)$d states of the next-nearest-neighbor transition-metal atoms. The study of nonlocal intersite hybrid excitations in transition-metal K-edge spectra allows for an examination of metal−metal interactions, which is important to better understanding the electrical and magnetic properties of transition-metal-bearing materials, particularly those that undergo metal−metal superexchange interactions.[20,35,36]

AUTHOR INFORMATION

Corresponding Author

*E-mail andrew.grosvenor@usask.ca; phone (306) 966-4660; fax (306) 966-4730.

ACKNOWLEDGMENT

The Natural Sciences and Engineering Research Council (NSERC) of Canada supported this work through a discovery grant awarded to A.P.G. The University of Saskatchewan is also thanked for supporting this work through a new-faculty start-up grant awarded to A.P.G. Mr. Thomas Regier, Mr. David Chevrier, Dr. Ning Chen, and Dr. Weifeng Chen of the Canadian Light Source (CLS) are thanked for help in carrying out XANES measurements at 11ID-1 and 06ID-1 at the CLS. The CLS is supported by NSERC, the National Research Council of Canada, the Canadian Institutes of Health Research, the Province of Saskatchewan, Western Economic Diversification Canada, and the University of Saskatchewan.

REFERENCES

(1) Wilke, M.; Farges, F.; Petit, P.-E.; Brown, G. E., Jr.; Martin, F. *Am. Mineral.* **2001**, *86*, 714.
(2) Farges, F.; Brown, G. E., Jr.; Rehr, J. J. *Phys. Rev. B* **1997**, *56*, 1809.
(3) Wong, J.; Lytle, F. W.; Messmer, R. P.; Maylotte, D. H. *Phys. Rev. B* **1984**, *30*, 5596.
(4) Westre, T. E.; Kennepohl, P.; DeWitt, J. G.; Hedman, B.; Hodgson, K. O.; Solomon, E. I. *J. Am. Chem. Soc.* **1997**, *119*, 6297.
(5) Waychunas, G. A.; Apted, M. J.; Brown, G. E., Jr. *Phys. Chem. Mineral.* **1983**, *10*, 1.
(6) Song, Y.; Zavalij, P. Y.; Suzuki, M.; Whittingham, M. S. *Inorg. Chem.* **2002**, *41*, 5778.
(7) Grosvenor, A. P.; Greedan, J. E. *J. Phys. Chem. C* **2009**, *113*, 11366.
(8) Gaultois, M. W.; Grosvenor, A. P. *J. Phys. Chem. C* **2010**, *114*, 19822.
(9) Gaultois, M. W.; Greedan, J. E.; Grosvenor, A. P. *J. Electron Spectrosc. Relat. Phenom.* **2010,** in press.
(10) Le Toquin, R.; Paulus, W.; Cousson, A.; Prestipino, C.; Lamberti, C. *J. Am. Chem. Soc.* **2006**, *128*, 13161.
(11) Grosvenor, A. P.; Cavell, R. G.; Mar, A. *J. Solid State Chem.* **2007**, *180*, 2702.
(12) Dräger, G.; Frahm, R.; Materlik, G.; Brümmer, O. *Phys. Status Solidi B* **1988**, *146*, 287.
(13) Glatzel, P.; Mirone, A.; Eeckhout, S. G.; Sikora, M. *Phys. Rev. B* **2008**, *77*, 115133.
(14) Petit, P. −E.; Farges, F.; Wilke, M.; Solé, V. A. *J. Synchrotron Rad.* **2001**, *8*, 952.
(15) Cabaret, D.; Joly, Y.; Renevier, H.; Natoli, C. R. *J. Synchrotron Rad.* **1999**, *6*, 258.
(16) Cabaret, D.; Bordage, A.; Juhin, A.; Arfaoui, M.; Gaudry, E. *Phys. Chem. Chem. Phys.* **2010**, *12*, 5619.
(17) Joly, Y.; Cabaret, D.; Renevier, H.; Natoli, C. R. *Phys. Rev. Lett.* **1999**, *82*, 2398.
(18) Uozumi, T.; Okada, K.; Kotani, A.; Durmeyer, O.; Kappler, J. P.; Beaurepaire, E.; Parlebas, J. C. *Europhys. Lett.* **1992**, *18*, 85–90.
(19) Frommer, J.; Nachtegaal, M.; Czekaj, I.; Weng, T.-C.; Kretzschmar, R. *J. Phys. Chem. A* **2009**, *113*, 12171.
(20) Vankó, G.; de Groot, F. M. F.; Huotari, S.; Cava, R. J.; Lorenz, T.; Reuther, M. arXiv: 0802.2744v1; 2008; p 1.
(21) Juhin, A.; de Groot, F.; Vankó, G.; Calandra, M.; Brouder, C. *Phys. Rev. B* **2010**, *81*, 115115.
(22) Glatzel, P.; Sikora, M.; Fernández-García, M. *Eur. Phys. J. Spec. Top.* **2009**, *169*, 207.
(23) Elfimov, I. S.; Anisimov, V. I.; Sawatzky, G. A. *Phys. Rev. Lett.* **1999**, *82*, 4264.
(24) Berry, F. J.; Holden, J. G.; Loretto, M. G. *J. Chem. Soc., Faraday Trans. I* **1987**, *83*, 615.
(25) Causa, M. T.; Tovar, M.; Obradors, X.; Labarta, A.; Tejada, J. *Phys. Rev. B* **1991**, *44*, 4455.
(26) Holland, T. J. B.; Redfern, S. A. T. *Mineral. Mag.* **1997**, *61*, 65–77.
(27) Denton, A. R.; Ashcroft, N. W. *Phys. Rev. A* **1991**, *43*, 3161.
(28) Shannon, R. D. *Acta Crystallogr., Sect. A* **1976**, *32*, 751.
(29) Thompson, A.; Attwood, D.; Gullikson, E.; Howells, M.; Kim, K.-J.; Kirz, J.; Kortright, J.; Lindau, I.; Pianetta, P.; Robinson, A.; Scofield, J.; Underwood, J.; Vaughan, D.; Williams, G.; Winick, H. *X-ray Data Booklet*; Lawrence Berkeley National Laboratory: Berkeley, CA, 2009.
(30) Ravel, B.; Newville, M. *J. Synchrotron Radiat.* **2005**, *12*, 537.
(31) Allred, A. L.; Rochow, E. G. *J. Inorg. Nucl. Chem.* **1958**, *5*, 264.
(32) Grosvenor, A. P.; Ramezanipour, F.; Derakhshan, S.; Maunders, C.; Botton, G. A.; Greedan, J. E. *J. Mater. Chem.* **2009**, *19*, 9213.
(33) Abbate, M.; de Groot, F. M. F.; Fuggle, J. C.; Fujimori, A.; Strebel, O.; Lopez, F.; Domke, M.; Kaindl, G.; Sawatzky, G. A.; Takano, M.; Eisaki, H.; Uchida, S. *Phys. Rev. B* **1992**, *46*, 4511.
(34) Bergmann, U.; Glatzel, P. *Photosynth. Res.* **2009**, *102*, 255.
(35) Chen, J. M.; Lee, J. M.; Huang, S. W.; Lu, K. T.; Jeng, H. T.; Chen, C. K.; Haw, S. C.; Chou, T. L.; Chen, S. A.; Hiraoka, N.; Ishii, H.; Tsuei, K. D.; Yang, T. J. *Phys. Rev. B* **2010**, *82*, 094442.
(36) Gaougoussis, C.; Calandra, M.; Seitsonen, A.; Brouder, Ch.; Shukla, A.; Mauri, F. *Phys. Rev. B* **2009**, *79*, 045118.